High quality-factor whispering-gallery mode in the photonic crystal hexagonal disk cavity

Han-Youl Ryu and Masaya Notomi

NTT Basic Research Laboratories, 3-1 Morinosato-Wakamiya, Atsugi 243-0198, Japan
hyryu@kaist.ac.kr

Guk-Hyun Kim and Yong-Hee Lee

Dept. of Physics, Korea Advanced Institute of Science and Technology, Daejeon 305-701, Korea

Abstract: We study whispering-gallery-like modes in photonic crystal air-bridge slab micro-cavities having *H*2 defects using finite-difference time-domain calculations. The defect geometry is optimized to increase the quality factor (*Q*) of the *H*2-cavity whispering-gallery mode (WGM). By symmetrically distributing 12 nearest neighbor holes around the defect and controlling size of holes, it is possible to drastically increase the *Q* of $>10^5$ while preserving effective mode volume of the order of the cubic wavelength in material. In addition, we investigate the effect of a dielectric circular post located around the center of the *H*2 cavity. This post can act as current and heat flow paths that promise electrically-pumped thermally-stable lasing operation. It is interesting to observe that the introduction of the post structure increases the *Q* of the WGM upto $4x10^5$ and the high *Q* $>10^5$ is still maintained even with large post size. Although diffractive out-coupling through the post is increased, radiated power outside the post is suppressed, which leads to large enhancement of the *Q* of the *H*2-cavity WGM.

OCIS codes: (230.5750) Resonators; (230.3990) Microstructure devices

References and links

1. H. Yokoyama, "Physics and Device Application of Optical Microcavities," Science **256**, 66-70 (1992).
2. O. Painter, R. K. Lee, A. Scherer, A. Yariv, J. D. O'Brien, P. D. Dapkus, and I. Kim, "Two-dimensional photonic band-gap defect mode laser," Science **284**, 1819-1821 (1999).
3. S. Noda, A. Chutinan, and M. Imada, "Trapping and emission of photons by a single defect in a photonic bandgap structure," Nature 407, 608-610 (2000).
4. H. Y. Ryu, H. G. Park, and Y. H. Lee, "Two-Dimensional Photonic Crystal Semiconductor Lasers: Computational Design, Fabrication, and Characterization," IEEE J. Sel. Top. Quantum Electron. **8**, 891-908 (2002).
5. J. Gérard and B. Gayral, "InAs quantum dots: artificial atoms for solid-state cavity-quantum electrodynamics," Physica E **9**, 131-139 (2001).
6. J. Vučković, M. Lončar, H. Mabuchi, and A. Scherer, "Design of photonic crystal microcavities for cavity QED," Phys. Rev. E **65**, 016608 (2001).
7. J. Vučković, M. Lončar, H. Mabuchi, and A. Scherer, "Optimization of the Q Factor in Photonic Crystal Microcavities," IEEE J. Quantum Electron. **38**, 850-856 (2002)
8. K. Srinivasan and O. Painter, "Momentum space design of high-Q photonic crystal optical cavities," Opt. Express **10**, 670-684 (2002), http://www.opticsexpress.org/abstract.cfm?URI=OPEX-10-15-670; K. Srinivasan and O. Painter, "Fourier space design of high-Q cavities in standard and compressed hexagonal lattice photonic crystals," Opt. Express **11**, 579-593 (2003), http://www.opticsexpress.org/abstract.cfm?URI=OPEX-11-6-579.
9. H. Y. Ryu, S. H. Kim, H. G. Park, J. K. Hwang, Y. H. Lee, and J. S. Kim, "Square-lattice photonic band-gap single-cell laser operating in the lowest-order whispering gallery mode," Appl. Phys. Lett. **80**, 3883-3885 (2002).

#3837 - $15.00 US Received 17 February 2004; revised 5 April 2004; accepted 6 April 2004

10. H. G. Park, J. K. Hwang, J. Huh, H. Y. Ryu, S. H. Kim, J. S. Kim, and Y. H. Lee, "Characterization of Modified Single-Defect Two-Dimensional Photonic Crystal Lasers," IEEE J. Quantum Electron. **38**, 1353-1365 (2002).
11. H. Y. Ryu, J. K. Hwang, and Y. H. Lee, "The Smallest Possible Whispering-Gallery-Like Mode in the Square Lattice Photonic-Crystal Slab Single-Defect Cavity," IEEE J. Quantum Electron. **39**, 314-322 (2003).
12. J. Vučković. And Y. Yamamoto, "Photonic crystal microcavities for cavity quantum electrodynamics with a single quantum dot," Appl. Phys. Lett. **82**, 2374-2376 (2003).
13. H. Y. Ryu, M. Notomi, and Y. H. Lee, "Very high quality-factor and small mode-volume hexapole modes in photonic crystal slab nano-cavities," Appl. Phys. Lett. **83**, 4294 (2003).
14. T. Baba, M. Fujita, A. Sakai, M. Kihara, R. Watanabe, "Lasing Characteristics of GaInAsP-InP Strained Quantum-Well Microdisk Injection Lasers with Diameter of 2-10 μm," IEEE Photon. Technol. Lett. **9**, 878-880 (1997).
15. C. Reese, B. Gayral, B. D. Gerardot, A. Imamoglu, P. M. Petroff, and E. Hu, "High-Q photonic crystal microcavities fabricated in a thin GaAs membrane," J. Vac. Sci. Technol. B **19**, 2749-2752 (2001).
16. C. Monat, C. Seassal, X. Letartre, P. Regreny, P. Rojo-Romeo, P. Viktorovitch, M. L. V. d'Yerville, D. Cassagne, J. P. Albert, E. Jalaguier, S. Pocas, and B. Aspar, "Modal Analysis and Engineering on InP-Based Two-Dimensional Photonic-Crystal Microlasers on a Si Wafer," IEEE J. Quantum Electron. **39**, 419-425 (2003).
17. S. L. McCall, A. F. J. Levi, R. E. Slusher, S. J. Pearton, and R. A. Logan, "Whispering-gallery mode microdisk lasers," Appl. Phys. Lett. **60**, 289-291 (1991).
18. M. Fujita, A. Sakai, and T. Baba, "Ultrasmall and Ultralow Threshold GaInAsP-InP Microdisk Injection Lasers: Design, Fabrication, Lasing Characteristics, and Spontaneous Emission Factor," IEEE J. Sel. Top. Quantum Electron. **5**, 673-681 (1999).
19. M. Cai, O. Painter, and K. J. Vahala, "Observation of critical coupling in a fiber taper to a silica-microsphere whispering-gallery mode system," Phys. Rev. Lett. **85**, 74-77 (2000).
20. A. F. J. Levi, S. L. McCall, S. J. Pearton, and R. A. Logan, "Room temperature operation of submicrometer radius disk lasers," Electron. Lett. **29**, 1666-1667 (1993).
21. R. E. Slusher, A. F. J. Levi, U. Mohideen, S. L. McCall, S. J. Pearton, and R. A. Logan, "Threshold characteristics of microdisk lasers," Appl. Phys. Lett. **63**, 1310-1312 (1993)
22. S. G. Johnson, S. Fan, A. Mekis, and J. D. Joannopoulos, "Multipole-cancellation mechanism for high-Q cavities in the absence of a complete photonic band gap," Appl. Phys. Lett. **78**, 3388-3390 (2001).
23. K. Nozaki, A. Nakagawa, D. Sano, and T. Baba, "Ultralow Threshold and Single-Mode Lasing in Microgear Lasers and Its Fusion With Quasi-Periodic Photonic Crystals," IEEE J. Sel. Top. Quantum Electron. **9**, 1315-1360 (2003).
24. H. Mabuchi and A. C. Doherty, "Cavity Quantum Electrodynamics: Coherence in Context," Science **298**, 1372-1377 (2002).
25. H. G. Park, S. K. Kim, S. H. Kwon, G. H. Kim, S. H. Kim, H. Y. Ryu, and Y. H. Lee, "Single-Mode Operation of Two-Dimensional Photonic Crystal Laser with Central Post," IEEE Photon. Technol. Lett. **15**, 1327 (2003).

1. Introduction

Resonant modes formed in photonic crystal micro-cavities with the high quality factor (Q) and small mode volume will find novel potential applications to integrated photonic devices[1-4] and quantum optics[5,6]. Several groups have reported the design of high-Q membrane-type photonic crystal slab cavities for the high $Q > 10^4$ together with effective mode volume of the order of the cubic wavelength in material ($(\lambda/n)^3$) [6-13]. Of these, resonant modes with characteristics of the whispering-gallery mode (WGM) have several interesting properties. The quadrupole mode in a square lattice[9,11] and the hexapole mode in a triangular lattice single-defect cavity[10,13] are good examples of the WGM formed in photonic crystal cavities. First, these modes show very high Qs. The finite-difference time-domain (FDTD) calculation shows that these mode can possess the Q of $>10^5$. In addition, unlike the WGM in micro-disk cavities, these photonic crystal WGMs are nondegenerate, which yields a large spontaneous emission factor and consequently low-threshold lasing operation. Furthermore, a dielectric post can be adopted for the current flow path in electrical pumping as in the case of micro-disk lasers [14]. Since there exists intensity node at the center of the WGM, the existence of the post structure does not degrade the Q of the mode [11].

In this paper, we study the WGM of photonic crystal disk cavities focusing on the so-called $H2$ cavities (formed by removing seven air holes) [15,16] using the FDTD calculation.

#3837 - $15.00 US Received 17 February 2004; revised 5 April 2004; accepted 6 April 2004

The WGM in these large-size cavities has some advantageous features compared with single-defect WGMs in view of real device applications. For example, the introduction of a post is technically much easier than in single-defect cavities and surface recombination loss, the major factor limiting low-threshold operation of single-defect lasers, could be significantly reduced due to enlarged cavity size. Although the cavity area is increased by several times compared with single-defect cavity cases, the mode volume is not so much increased because the mode is mainly distributed around the cavity boundary. One important issue that should be addressed is how large Q values can be achieved in the WGM of the photonic crystal disk cavities. So, our main objective in this work is to increase the Q of the WGM by optimizing cavity structures. In fact, WGMs in disk cavities other than single-defect cavities have relatively low Q values as will be mentioned in Section 2. Therefore, we propose and optimize modified $H2$ defect cavities to increase the WGM of the cavity in Section 3. Over 100-fold enhancement of the Q and hence Qs of $>10^5$ will be numerically demonstrated. In section 4, effects of dielectric posts placed around cavity center are investigated for real application of our proposed structures, and results on the Q enhancement in the $H2$-cavity WGM with post structures are presented.

We used the FDTD method for the calculation of resonant mode properties such as field distributions, resonant frequencies, and Q. In our FDTD calculation, perfectly-matched-layer boundary conditions are employed. Lattice constant (a) is discretized to 20 mesh points. In most cases, the calculation domain includes 15x15 unit cells in the horizontal plane and 6 unit cells in the vertical direction. Symmetry conditions are imposed in all directions to save computational efforts. The total Q is decomposed into the horizontal and the vertical Q components, and the vertical Q is regarded as the ultimate Q to be achieved because the vertical Q approaches the total Q when the computational domain is sufficiently large. The position that separates the vertical radiation from the slab-guided in-plane loss is chosen to be 0.5 a from the slab surface [9]. In this separation boundary, we confirmed the convergence of the total Q toward the vertical Q. Therefore, we regard the vertical Q as the genuine Q of a resonant mode assuming the horizontal Q is infinity. In all calculations, thickness of the air-bridge slab is fixed to 0.6 a, and the refractive index of a slab material is chosen to be 3.4.

2. WGM in photonic crystal disk cavities

Although the WGM is usually observed and referred in micro-disk and micro-sphere cavities [17-19], whispering-gallery-like modes formed in photonic crystal defect cavities also have characteristics similar to the micro-disk WGMs [9,11]. For example, both electric and magnetic fields form standing wave patterns along the cavity boundary. It results in a null of electromagnetic energy at the center. Polarization of electric fields for transverse-electric modes is also directed radially. In this sense, the quadrupole mode of the square lattice single-defect and the hexapole mode of the triangular lattice single-defect are regarded as the photonic crystal WGM with the azimuthal mode number of 2 and 3, respectively [9,13]. The electric field intensity distributions of WGMs in large-size defect cavities are presented in Fig.

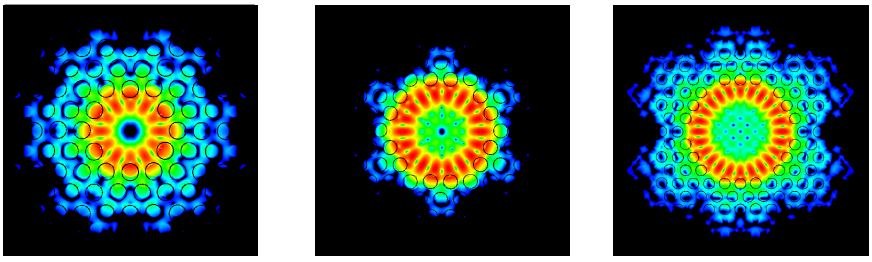

(a) (b) (c)

Fig. 1. Whispering-gallery mode (WGM) in photonic crystal hexagonal disk cavities. (a) $H2$-cavity WGM, (b) $H3$-cavity WGM, (c) $H4$-cavity WGM.

#3837 - $15.00 US Received 17 February 2004; revised 5 April 2004; accepted 6 April 2004

1. Each disk-type defect cavity in Fig. 1(a), (b), and (c) is often called the *H*2 cavity, the *H*3 cavity, and the *H*4 cavity [15,16]. Size of the *H*2-cavity is comparable to that of the smallest microdisk lasers [18,20]. Field patterns of these photonic crystal WGMs are quite similar to those of the micro-disk WGM. In the WGM of hexagonal photonic crystal cavities, the number of high-intensity lobes is equal to the number of neighboring holes around the cavity. Each WGM in the *H*2, *H*3, and *H*4 cavity can be classified as the mode with the azimuthal mode number of 6, 9, 12, respectively.

Despite the similar mode distributions, the origin of a high *Q* from the photonic crystal WGM and the micro-disk WGM is different. In case of the micro-disk WGM, the optical loss is dominated by radiation losses determined by total internal reflection at disk boundary. In this case, the WGM with a higher-order mode number formed in a large-size disk cavity exhibits a high *Q* [17,21]. Therefore, it is difficult to obtain the high-*Q* and small mode volume simultaneously from the micro-disk cavity. In case of the photonic crystal WGM, however, out-of-plane radiation is a main optical loss channel because in-plane propagation is restricted by the photonic band gap. The out-of-plane radiation in photonic crystal resonant modes is closely related to the mode pattern. In a certain symmetrically distributed mode pattern, the vertical radiation can be suppressed by destructive interference or far-field cancellation effects [8-11,22]. The high-*Q* of the single-defect WGMs is largely benefited from the well symmetrized mode distribution [11,13].

The *Q* of each WGM is plotted as a function of air-hole radius in Fig. 2. The *Q* of the *H*2-cavity WGM is only several hundred and that of the *H*4-cavity WGM is less than 10^4 at best. These *Q* values are much smaller than those of single-defect WGMs despite increased cavity size. So, WGMs of these photonic crystal disk cavities are not so advantageous to the micro-disk WGMs in terms of the *Q*. The low-*Q* of these modes can be interpreted by the symmetry argument. The WGM of the *H*2 cavity, for example, has 12 high-intensity lobes along the cavity boundary. Since 6 lobes lies in the Γ-M direction and other 6 ones lies in the Γ-K direction, each adjacent lobe shows different shape and intensity. That is, the 12 lobes in the *H*2 WGM are not distributed symmetrically because this mode pattern is not symmetry-matched with the basic 6-fold symmetry of the triangular lattice. This results in poor cancellation effect in far fields and consequently low *Q*s. Figure 3 shows the Fourier-space field intensity (a) and the side-view of real-space electric field intensity (b) of the *H*2 cavity WGM. The Fourier-space field distribution is obtained by the Fourier transform of real-space field components just above the slab surface [7,8]. In Fig. 3(a), the black circle indicates light line inside which field components contribute out-of-plane radiation. Relatively high intensity inside the light line implies that this mode undergoes large radiation loss as one can see from Fig. 3(b).

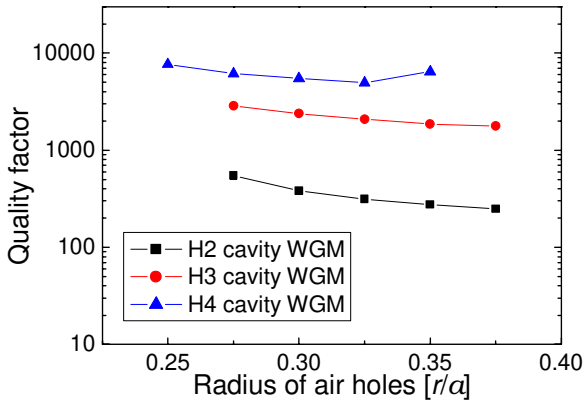

Fig. 2. Quality factor (*Q*) of the WGM for *H*2, *H*3, and *H*4 disk cavities versus radius of air holes.

#3837 - $15.00 US
Received 17 February 2004; revised 5 April 2004; accepted 6 April 2004

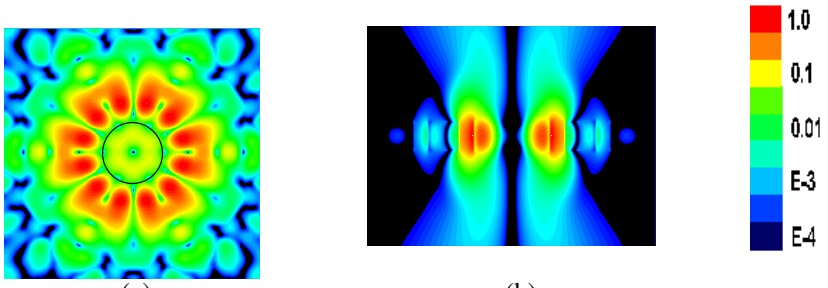

(a) (b)

Fig. 3. (a) Fourier-space electric field intensity distribution. Black circle represents light line. (b) Side-view electric field intensity of the WGM in Fig. 1(a). A color map of relative intensity scale is shown at the right of (b).

3. Optimization for the high-*Q* WGM in the *H*2 defect cavity

In this section, the *H*2 cavity structure is modified in order to reduce radiation loss of the WGM. First, it is believed that the WGM should exhibit a higher *Q* if the 12 high-intensity lobes are made to be distributed symmetrically. Because high-intensity regions of the mode exist along 12 nearest neighbor holes, the lobes would be distributed more symmetric if the 12 nearest neighbor holes are positioned symmetrically. To see this effect, 6 nearest neighbor holes in the Γ-M direction are pushed away along the radial direction as shown in Fig. 4(a). If the displacement of 6 holes, *p* is equal to $(2 - \sqrt{3})\ a$, the 12 nearest neighbor holes are symmetrically distributed, which means the distance from the defect center to each hole is all the same and the separation between adjacent nearest neighbor holes is also equal. The effect of such modification appears in Fig. 4(b) where the *Q* is plotted as a function of the displacement parameter, *p* when air-hole radius is 0.3 *a*. Rapid increase of a *Q* with *p* is observed until *p* reaches $(2 - \sqrt{3})\ a$, where the symmetric distribution condition for 12 nearest holes is perfectly satisfied. Here, the *Q* is as large as 75000 that is more than 100 times higher than that the unmodified structure. In this way, our symmetry argument is successfully applied

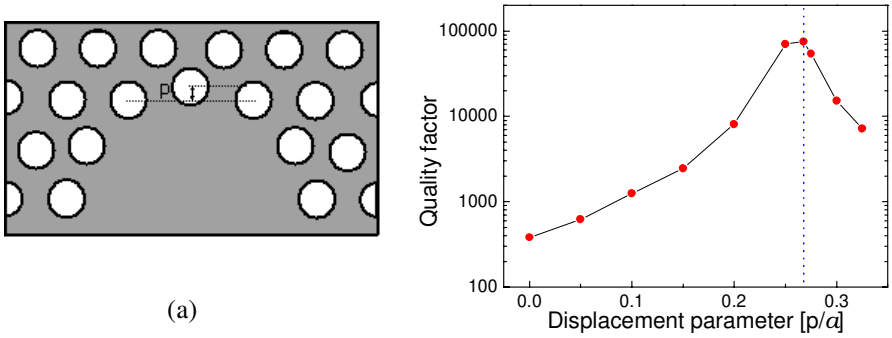

(a) (b)

Fig. 4. (a) Configuration of the modified *H*2 cavity. Here, nearest neighbor holes along the Γ-M direction are pushed away along the radial direction by the displacement parameter, *p*. (b) Quality factor as a function of *p* when radius of holes is 0.3 *a*. The blue dotted line indicates the position where nearest neighbor holes are symmetrically distributed.

#3837 - $15.00 US
Received 17 February 2004; revised 5 April 2004; accepted 6 April 2004

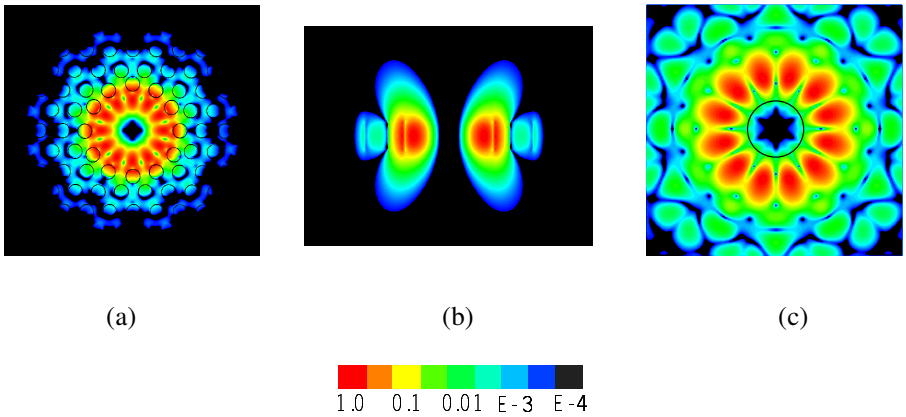

Fig. 5. Electric field intensity ($|E|^2$) distribution of the WGM in a structure shown in Fig. 4(a).. A color map of relative intensity scale is shown at the bottom of figures. (a) $|E|^2$ at the center plane of the slab. Circles represent air holes (b) Side view of the $|E|^2$, (c) Fourier space representation. The black circle near center indicates light line.

to the Q optimization of the $H2$ cavity WGM. Electric field intensity patterns in real space and Fourier space are shown in Fig. 5 when p is $(2 - \sqrt{3})\ a$. Field intensity inside the slab plane shows that 12 high-intensity lobes exhibit identical shape and intensity, which results in suppressed out-of-plane radiation as shown in Fig. 5(b) and week Fourier intensity components inside light line in Fig. 5(c). The 12 lobes of dominant Fourier intensity components also show 12-fold symmetrical patterns unlike 6-fold distribution of the unmodified case in Fig. 3(b).

Next step for the Q optimization is to modify the radius of 12 nearest neighbor holes (r_m) as shown in Fig. 6(a). From now, the p value is fixed to be $(2 - \sqrt{3})\ a$. Since these nearest holes affect mode profiles significantly, resonant frequencies should be changed much by this modification. Fig. 6(b) shows resonant frequencies as a function r_m for three regular hole radius (r), 0.275 a, 0.3 a, and 0.325 a. The resonant frequency varies on a large scale as r_m changes, whereas it hardly varies with r. This result implies that frequency tuning of the

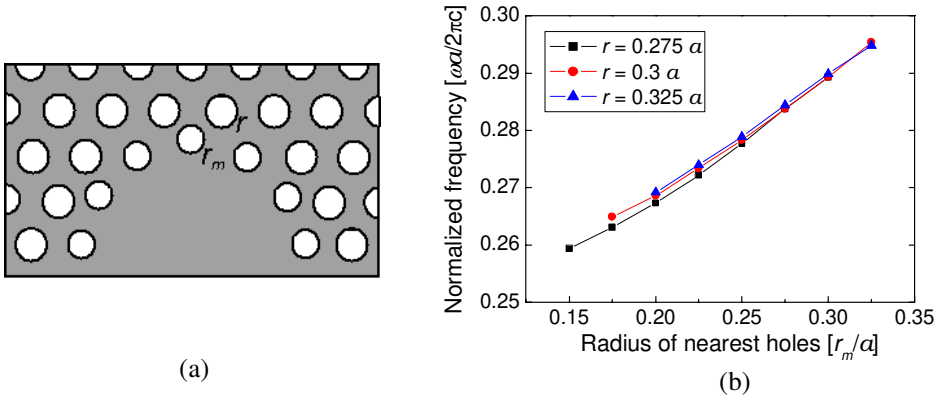

Fig. 6. (a) Configuration of the modified $H2$ cavity from the structure in Fig. 4(a) with $p = (2 - \sqrt{3})\ a$. Here, radius of nearest neighbor holes is modified from r to r_m. (b) Quality factor as a function of r_m for three r values.

#3837 - $15.00 US
Received 17 February 2004; revised 5 April 2004; accepted 6 April 2004

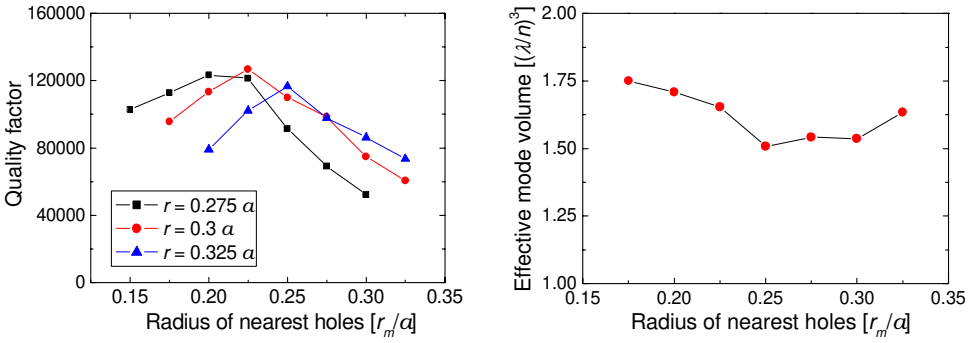

(a) (b)

Fig. 7. (a) Quality factors as a function of r_m for three r values in the structure, Fig. 6(a). (b) Effective mode volume of the WGM as a function of r_m when radius of holes is 0.3 a.

WGM can be performed effectively by modifying only nearest neighbor holes. Since the regular holes outside the nearest holes determine the frequencies of a photonic band gap, the r and the r_m respectively control the band gap frequencies and the resonant mode frequency almost independently. Next, the Q of the WGM is calculated as a function of r_m for three values of r in Fig. 7(a). By this modification, the highest Q of >120000 is obtained when r is 0.3 a and r_m is 0.225 a. Note that the Q does not change rapidly with r or r_m. High Qs > 50000 are preserved in wide ranges of r and r_m. So, we expect slight variation or fluctuation of structural parameters do not degrade the Q significantly. Because the high Q region covers a wide frequency range, the WGM of this modified $H2$ cavity can be advantageously used for WDM applications of lasers and optical filters.

In addition to the Q, we calculate the mode volume of the $H2$ WGM. In Fig. 7(b), the effective mode volume is plotted as a function of r_m when r is 0.3 a. The effective mode volume for cavity quantum electrodynamics (CQED) is defined as the ratio of total electric field energy to the maximum of the electric field energy density [2]. It is 1.5 ~ 1.8 $(\lambda/n)^3$ where λ and n are mode wavelength and refractive index of material, respectively. This mode volume is about 2~3 times larger than that of single-defect resonant modes. However, remembering that the $H2$ cavity is formed by removing 7 air holes, the mode volume of the $H2$-cavity WGM is not so much increased. Due to the high Q and small mode volume, one can anticipate large CQED effects from this mode. For example, the Purcell factor[5] is estimated to be as large as 5000. So, we expect the modified $H2$-cavity WGM can find potential application to future quantum information technology [24].

The temporal variation of electric field intensity and magnetic field amplitude is shown in Fig. 8 when r is 0.3 a and r_m is 0.225 a. Fields are concentrated around the cavity boundary and show very week intensity near the cavity center, $<10^{-4}$ of the highest intensity in all time sequence. Since high intensity regions exist in only limited area, the mode volume is small compared to the cavity volume. Good lateral mode confinement also contributes to the small mode volume. Field intensity outside the cavity region exponentially decreases very rapidly. In addition, due to the pushed and reduced nearest air holes, the overlap of high field intensity region with dielectric material is improved compared to the unmodified case in Fig. 1(a). And, the mode volume of the modified WGM is almost unchanged from the case of the unmodified H2-cavity structure although the cavity area is a little enlarged.

Further Q optimization could be performed by the modification of the second or the third nearest neighbor holes. However, these modifications are more complicated and the achieved Qs ~ 10^5 by previous optimization is sufficiently large for many applications. So, we do not

#3837 - $15.00 US
Received 17 February 2004; revised 5 April 2004; accepted 6 April 2004

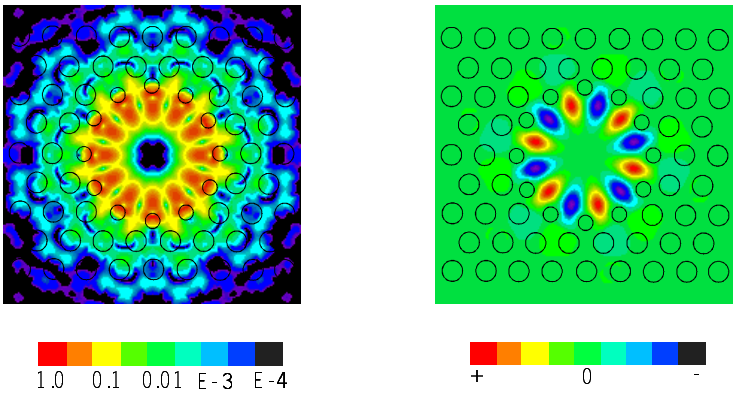

Fig. 8. (a) (330kB) Movie of electric field intensity of the modified *H*2-cavity WGM (b) (90kB) Movie of magnetic field amplitude of the modified *H*2-cavity WGM. Regular hole radius and modified hole radius are 0.3 *a* and 0.225 *a*, respectively. Black circles represent air holes.

go further. And, similar optimization schemes can also be applied to WGMs of the *H*3 and *H*4 cavities.

Note that the proposed cavity structures in this section are similar to micro-gear lasers and quasi-periodic photonic crystal cavities which have been proposed by Prof. Baba's group. Both structures employ rotationally symmetric corrugations along the cavity boundary, which results in nondegenerate high-Q WGMs. However, our structures are based on photonic crystals unlike micro-gear or quasi-periodic structures. So, one can utilize properties of the photonic band gap. For example, the WGM can be coupled to other photonic crystal elements such as photonic crystal waveguides and can be used as a cavity mode in the add-drop filter system.

4. Effect of post structures on the *Q* of the WGM

In this section, we investigate the effect of a dielectric post placed around the center of the cavity on the *Q* of the *H*2-cavity WGM. The introduction of the post results in at least three advantageous features for the application to semiconductor lasers. First, current injection through the post can be feasible. Second, thermally stable operation is expected since the post will also act as a heat sink path. This property will result in the realization of continuous-wave

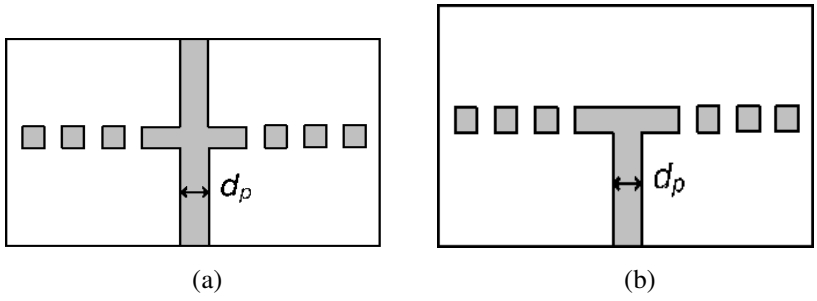

Fig. 9. Side –view of dielectric post structures. d_P means post diameter. Here, d_P is about 1.0 *a*. (a) Symmetric slab, (b) Asymmetric slab.

#3837 - $15.00 US
Received 17 February 2004; revised 5 April 2004; accepted 6 April 2004

operation of photonic crystal lasers. Third, single mode operation would be achieved if other modes are discouraged by the existence of the post. Very recently, single-mode lasing operation with good thermal property has been experimentally demonstrated by the KAIST group [25]. All these important properties could be utilized only when the post doesn't degrade the Q of the WGM significantly. Because the WGM has node of electromagnetic field near the center, it is expected that the presence of the post hardly affect the Q of the WGM as have been verified from the square lattice single-defect WGM [11]. We consider two types of post structures, symmetric post and asymmetric post. Each post is schematically drawn in Fig. 9. Actually, the asymmetric post is more realistic since fabrication of this structure type is not so difficult. Although the realization of the symmetric post is technically challenging, this type is also investigated because the top post might act as an electrode contact as in the case of micro-disk lasers.

4.1 Symmetric post

First, we calculated the change of resonant frequencies when the post is introduced and observed a very small shift of the resonant frequency. When post diameter, d_P is increased upto 2.0 a, the resonant frequency decreases by less than 1%. This frequency stability originates from the fact that mode distribution is not so much affected by the post because of intensity node around cavity center. In addition, effective mode volume is also hardly changed. Next, the Q is calculated and plotted as a function of post diameter in Fig 10. In this calculation, r and r_m are fixed to be 0.3 a and 0.225 a, respectively. The refractive index of the dielectric post is the same as that of slab material, 3.4. Surprisingly, the Q increases considerably when the post is introduced. When d_P is 1.0 a, the Q is >400000 that is about 3.5 times larger than the Q without a post. In this case, the Purcell factor is even higher than 20000. Still large Q ~ 200000 is observed even with quite large post diameter ~ 2.0 a. This result is contrary to simple expectation that diffractive out-coupling through the post would deteriorate the Q of this mode. This peculiar behavior has not been observed in other cases such as single-defect WGMs or micro-disk WGMs. Large Q enhancement by posts is a unique property of the modified $H2$-cavity WGM.

In order to understand this result, the Poynting vector is calculated when d_P is 0 and 1.0 a as displayed in Fig. 11. This figure shows temporal variation of the Poynting vector at the vertical plane z = 2.3 a measured from center of the slab. Since the slab thickness is 0.6 a, the distance from the Poynting vector calculation plane and slab surface is 2.0 a. So, it represents only radiated power out of the photonic crystal slab and accounts for the difference between calculated Qs of the WGM with and without a post. The calculation plane size is 13.0 a x 13.0

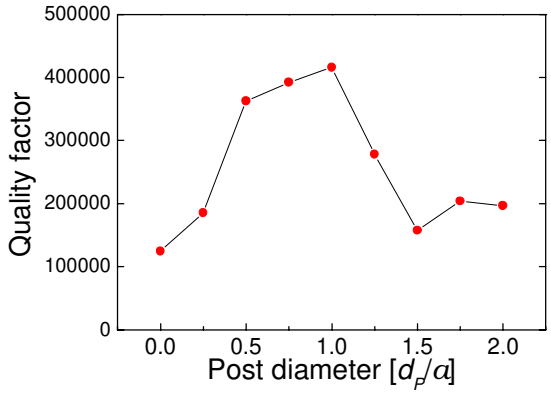

Fig. 10. Quality factors of the WGM with the symmetric post plotted as a function of post diameter. Regular hole radius and modified hole radius are 0.3 a and 0.225 a, respectively.

#3837 - $15.00 US Received 17 February 2004; revised 5 April 2004; accepted 6 April 2004

a, which covers angular range from -85 degree to +85 degree. When there is no dielectric post, six high-intensity Poynting vector lobes appear, which is reminiscent of the basic six-fold symmetry of the hexagonal structure. This implies that 12 symmetrical nearest neighbor holes are not so much responsible for optical loss and outer regular holes mainly contribute to radiation loss. In addition, Poynting vectors are distributed relatively uniformly over wide angular range in this case. In Fig. 11(b) where the dielectric post is employed, large Poynting vector components are observed near the post, which implies optical loss is dominantly coupled through the post. Actually, the Poynting vector is strongest near the boundary of the post not inside the post. At the same time, radiated power outside the post is much decreased compared to the case without a post. Six dominant Poynting vector components in Fig. 11(a) are almost disappeared and Poynting vectors with large angular components measured from the normal are also much suppressed, which results in higher *Q*s from the post-type WGM. After all, introduction of the post reduces optical loss by out-coupling radiation fields mainly through the post while suppressing optical radiation outside the post. However, the fundamental reason why the addition of the post tends to increase the Q is not clearly understood in this present work, and it will be treated in the future work.

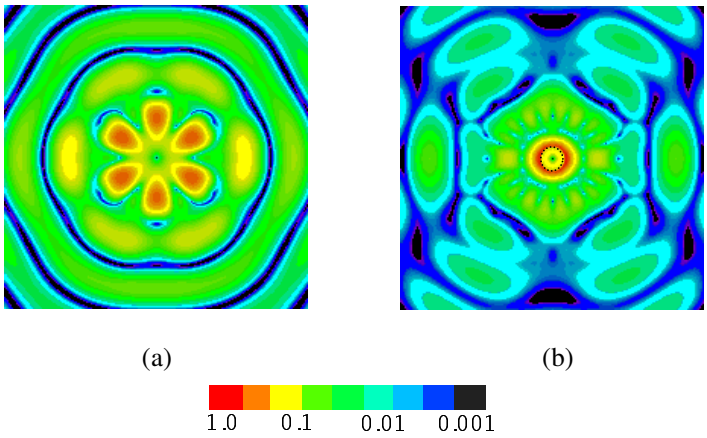

Fig. 11. (a) (340kB) Movie of the Poynting vector calculated at z = 2.3 a when there is no post. (b) (270kB) Movie of the Poynting vector when the post diameter is 1.0 a. A dotted circle near the center indicates the post.

4.2 Asymmetric post

The Q of the WGM in the asymmetric post structure shown in Fig. 9(b) is calculated in Fig. 12(a). Here, r and r_m are the same as in the previous subsection, 0.3 a and 0.225 a, respectively. Still, the Q is higher compared to the Q without the post. However, the amount of Q enhancement is smaller than that in the symmetric post case. The largest Q is ~180000 when d_P is 1.0 a. The Q is decomposed into the top component (Q_{top}) and the bottom component (Q_{bottom}). Each Q component represents optical loss into the air above the slab and into the slab bottom where the post is located, respectively. Decomposed Qs are plotted in Fig. 12(b). The behaviors of Q_{top} and Q_{bottom} are not so regular with post diameter. Q_{top} is higher than Q_{bottom} when d_P is <0.5 a or >1.5 a, which means optical loss into the bottom post direction is larger. However, when d_P is near 1.0 a, optical loss into the top air direction is larger than the loss into the bottom. This implies that more optical output is collected above the slab surface in this case. So, one can control the optical out-coupling efficiency depending on the post size. Poynting vectors calculated above and below the slab are shown in Fig. 13 when d_P is 1.0 a. Fig. 13(a) and (b) show temporal variation of the Poynting vector at the horizontal plane z = 2.3 a and z = -2.3 a, respectively. Main characteristics of Poynting

#3837 - $15.00 US
Received 17 February 2004; revised 5 April 2004; accepted 6 April 2004

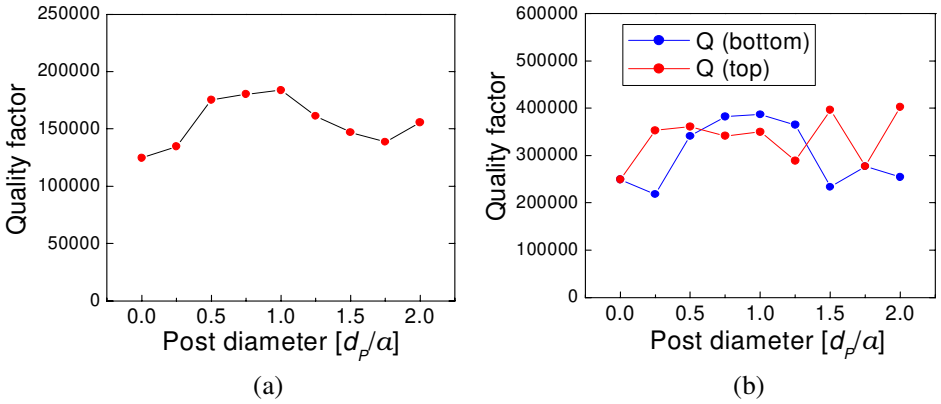

Fig. 12. (a) Quality factor of the WGM with asymmetric posts versus post diameter. (b) Quality factor decomposed into the top and the bottom components. Each represents optical loss into the top air region and the bottom post region, respectively.

vectors are similar to the case of symmetric posts in Fig. 11. However, the Poynting vector around the post is relatively higher in the asymmetric case as shown in Fig. 13(b). So, the post acts as a main optical loss channel. Nevertheless, radiated power outside the post is still low compared to the above-slab radiation. This results in lower optical loss into the slab bottom direction when the asymmetric post diameter is 1.0 a.

As mentioned previously, the preservation of a high Q for the large post diameter is advantageous to single mode operation through the suppression of other resonant modes. The Q of the other modes whose resonant frequency is close to the WGM is decreasing rapidly as post diameter increases. When d_P is larger than 1.0 a, the Q of these neighboring modes drops below 1000. So, more than 100-fold Q-distinction ratio can be achieved, which should lead to stable single-mode operation.

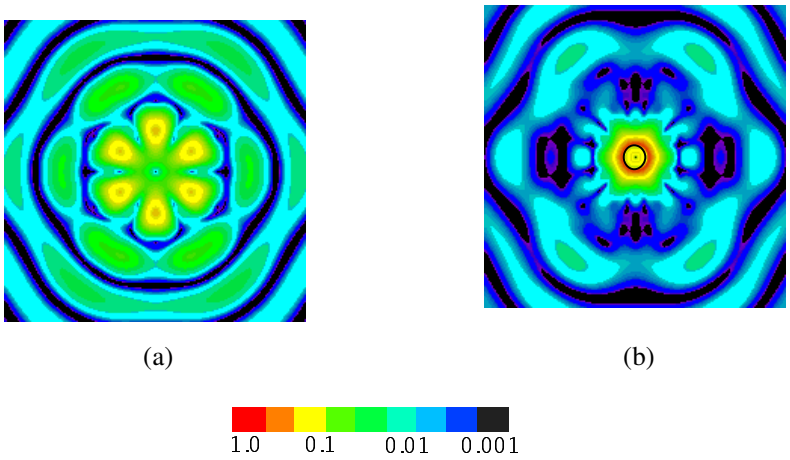

Fig. 13. (a) (300kB) Movie of the Poynting vector calculated at z = 2.3 a where there is no post. (b) (310kB) Movie of the Poynting vector calculated at z = -2.3 a where there is a post with diameter of 1.0 a. A dotted circle near the center indicates the post.

#3837 - $15.00 US
Received 17 February 2004; revised 5 April 2004; accepted 6 April 2004

5. Summary

In this paper, we numerically study the whispering-gallery-like mode formed in a photonic crystal slab *H*2 disk cavity. This mode can be classified as the WGM with the mode number of 6. Based on mode symmetry and far-field cancellation arguments, we optimize the *Q* of the *H*2 cavity WGM. By modifying only nearest neighbor holes so that 12 high-intensity lobes can be distributed symmetrically, over 100-fold enhancement of the *Q* is achieved. High *Q*s > 50000 are observed over a wide parameter space of air holes radius, which is useful for frequency tuning of the WGM without large change of *Q*s. The *Q* increases still further by employing a post around cavity center. The $Q > 4 \times 10^5$ is obtained from the WGM having symmetrical posts below and above the air-bridge slab cavity. Introduction of the post reduces total optical loss by out-coupling radiation fields mainly through the post while suppressing optical radiation outside the post. By combining our proposed WGM with the dielectric post, we expect the realization of single-mode electrically-pumped thermally-stable operation of photonic crystal semiconductor lasers. Throughout all modification processes, small effective mode volume, ~1.5 $(\lambda/n)^3$ is preserved. Due to high-*Q* and small mode volume, very large Purcell factor ~20000 is theoretically achievable. Therefore, we also expect applications of the proposed WGM to quantum optical devices.

#3837 - $15.00 US Received 17 February 2004; revised 5 April 2004; accepted 6 April 2004